JOURNAL OF MATERIALS SCIENCE 31 (1996) 1035–1042

Melt-extracted oxide ceramic fibres – the fundamentals

M. ALLAHVERDI, R. A. L. DREW, J. O. STROM-OLSEN*
*Department of Mining and Metallurgical Engineering and *Center for the Physics of the Materials, Physics Department, McGill University, Montreal, PQ, Canada*

A melt-extraction technique, using a sharpened molybdenum wheel, has been used to produce fine oxide ceramic fibres. Wetting of the molybdenum wheel by molten ceramic is a key parameter in the melt-extraction process. Two types of fibre are generally obtained, depending on the extraction speed. At very low wheel speed, fine and uniform fibres of high quality are produced. However, when the wheel speed exceeds a critical velocity, Rayleigh waves are formed on the free surface of the fibres. Moreover, the average fibre thickness first increases with the wheel velocity, then passes through a maximum, decreasing at high velocity. This thickness variation is discussed in terms of both surface tension and viscosity of the liquid ceramics.

1. Introduction

The demand for materials with high mechanical and thermal performance has led to the development of metal– and ceramic–matrix composites (MMCs and CMCs). Incorporation of fibres (continuous and discontinuous) in MMCs and CMCs improves the physical and mechanical properties of monolithic metal alloys and ceramics.

Ceramic fibres can exhibit good mechanical properties (e.g. high tensile strength and elastic modulus) and favourable physical and chemical properties (e.g. low density, inertness, and high oxidation resistance at elevated temperatures). Fibres such as Al_2O_3, SiC, and carbon have been used to improve the properties of metal alloys, ceramics, and glasses [1].

Various methods have been used to make ceramic fibres, such as chemical vapour deposition (CVD), sol–gel methods, slurry spinning and fibre drawing [2]. Rapid solidification technology (RST), e.g. melt extraction, can also be used to produce both ribbon and fibre. An advantage of RST is that the fibres are produced directly from the melt.

Melt extraction was developed in 1974 by Maringer *et al.* for the production of metal fibres [3–5]. They divided the technique into crucible melt extraction (CME) and pendant drop melt extraction (PDME) as shown in Fig. 1. The method (in one or other of its forms) was successful in making amorphous or crystalline metallic fibres. For example, large numbers of amorphous iron-based alloys, steel, titanium and its alloys, etc., have been extracted from their corresponding melts [6]. However, there have been few attempts to produce ceramic fibres using CME or PDME [7–9]. Schwartzkopf *et al.* [7, 8] used the PDME method to produce superconducting oxide fibres of compounds containing yttrium, barium, copper, and strontium oxides. No structural application has ever been sought for melt-extracted ceramic fibres. The CME method was also used to produce thick fibres or ribbon-like products of some oxide ceramics [9]. The main difficulty involved in the melt-extraction of ceramics is their very high melting temperatures and associated problems, such as oxidation, dissociation, and severe reactions with the containment material at elevated temperatures.

Recently, we have reported [10] a development of the melt extraction process which proved capable of producing very high-quality fibres of oxide ceramics with diameters down to 5 μm. The resulting materials have high fracture strength (up to 6 GPa) and, frequently, exceptional flexibility. The process is, therefore, very promising for producing ceramic fibres for reinforcement. In the present article we examine in more detail, the way in which the parameters of the extraction process control the morphology and microstructure of oxide fibres.

2. Experimental procedure

Fig. 2 shows a schematic illustration of the melt-extraction system used. The extracting wheel is a disc of molybdenum with a very sharp tip (wheel tip radius $\leqslant 20$ μm). Initially, oxy-propane and oxy-acetylene torches were used to melt a sintered pellet of a desired mixture of oxide ceramics (Fig. 2a). To increase the melt temperature, improve the control of the melt stability, and provide brief contact with the molybdenum wheel tip, a 150 W CO_2 laser beam was used with the sample in the form of an extruded rod which was fed slowly on to the wheel edge (Fig. 2b).

For the present work, four combinations of oxide ceramics were studied, as shown in Table I. Eutectic compositions were selected due to lower melting points and their stronger tendency to become

0022–2461

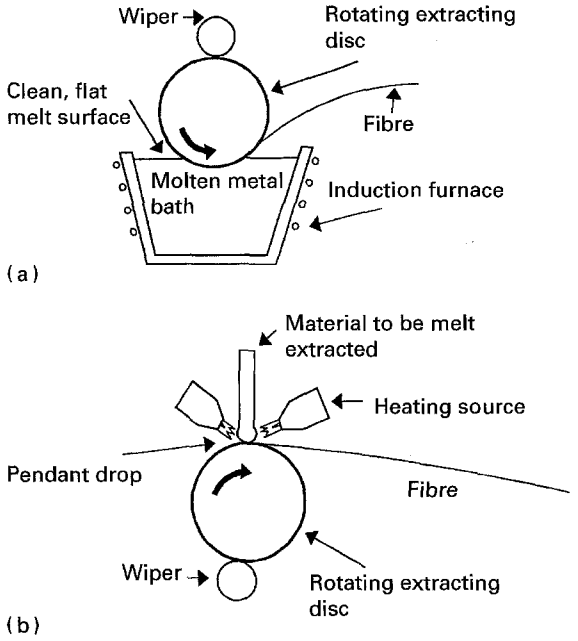

Figure 1 Schematic drawings of (a) crucible melt extraction (CME) and (b) pendant drop melt extraction (PDME) techniques.

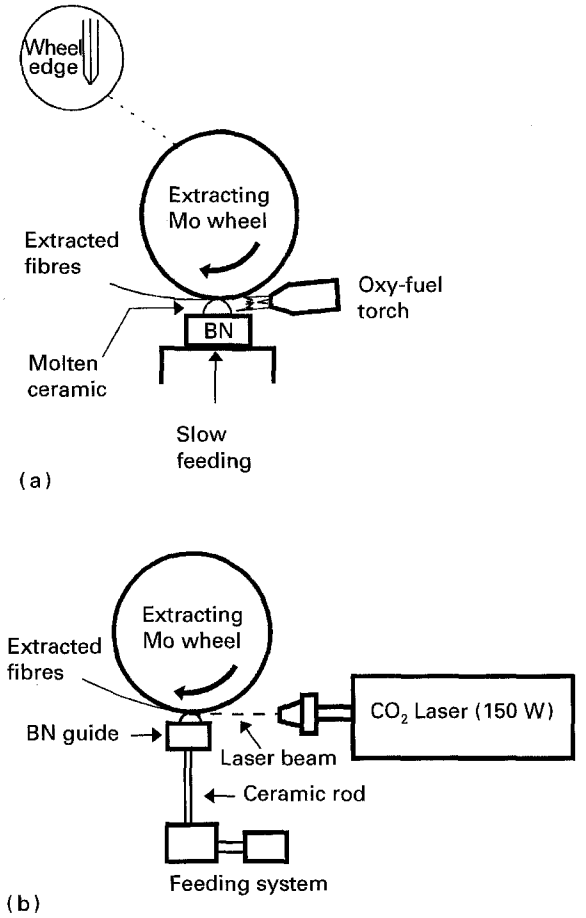

Figure 2 Schematic drawings of melt extraction using (a) oxy-fuel torch and (b) a CO_2 laser.

amorphous. Mixtures of oxide powders were initially attrition milled for 2 h with water and alumina media (because CaO reacts with water, iso-propanol was used as a fluid for attrition milling of $CaO–Al_2O_3$ powders). Then, the prepared slurry was dried in a microwave oven. The powder was either die-pressed into 5 mm diameter pellets or extruded into 2.5 mm diameter rods. A plasticizer (8 wt % starch) was added together with water to aid the extrusion process. The extruded ceramic was dried for 24 h at room temperature. In both cases, sintering was performed at 1500 °C for 1 h in air.

Before starting extraction, a sintered rod was placed inside a BN guide, attached to the feeding system and melted by the laser (see Fig. 2b). After forming a liquid droplet just beneath the wheel tip, the molten drop was slowly brought into contact with the rotating wheel by feeding the rod at a speed of 3 mm min^{-1} (almost 15 mm^3 min^{-1}). It should be noted that the laser power was insufficient to melt the ceramic rod when the feed rate was increased to high values. Therefore, to maintain the melt temperature constant, only one feeding rate (3 mm min^{-1}) was used for all extraction velocities. Various extraction rates were examined with tangential wheel speeds in the range of 1–65 m s^{-1}. Ceramic fibres were then extracted under appropriate conditions.

A key parameter in controlling the quality of fibres extracted is the wetting of the molybdenum wheel by the molten ceramic. The wetting behaviour in the melt-extraction technique is different from that found in a conventional wetting test, such as the sessile drop test. Therefore, a test was designed which partially simulates the transient wetting behaviour of the hot liquid ceramic in contact with a cold molybdenum surface. A small bead (~2 mm diameter) of the sintered oxide ceramics was placed on top of a 1 μm polished molybdenum plate. The sample was quickly melted after being exposed to the laser beam. The molten ceramic formed a tiny spherical drop. Laser heating was only continued for approximately 5 s after which the laser was turned off and the drop rapidly solidified. A contact angle formed at the contact surface with the molybdenum substrate. Fig. 3 shows a schematic drawing of the apparatus. The sample (glued to a plate) was examined with an optical microscope equipped with a calibrated vernier stage in order to measure the contact angle.

The temperature of the molten drop was measured by an infrared pyrometer (Minolta/Lands Cyclops 52)

TABLE I Composition of oxide ceramics studied

Compounds	Wt % (mol %)	Approximate melting temperature (°C)
$CaO–Al_2O_3$ (CA)	35.2–64.8 (50–50)	1600
$ZrO_2–Al_2O_3$ (ZA)	42.6–57.4 (38–62)	1890
$ZrO_2–Al_2O_3–SiO_2$ (ZAS)	31–53–16 (24.3–50–25.7)	1780
$ZrO_2–Al_2O_3–TiO_2$ (ZAT)	44–42–14 (37.8–43.6–18.6)	1610

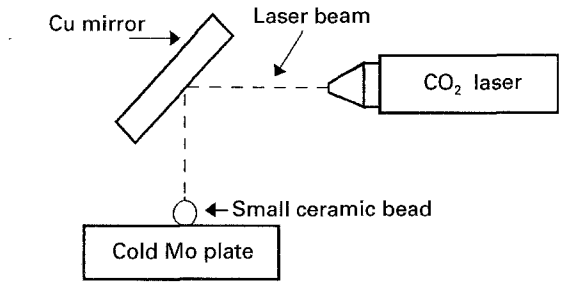

Figure 3 Schematic drawing of the wetting test apparatus.

assuming an emissivity of 0.3. Measuring the temperature was crucial, but difficult, due to the very small size of the droplet (~4 mm diameter) and uncertain emissivity of the oxide systems studied.

Melt-extracted fibres were studied by optical microscopy and scanning electron microscopy (SEM, Jeol-JSM 840A) to investigate the fibre geometry and morphology. For the SEM study, crushed fibres were placed on carbon adhesive tape and then coated with Au/Pd using a sputter coater. The degree of crystallinity of fibres was examined by XRD (Phillips diffractometer APD1700) of crushed fibres using CuK_α radiation (at 40 kV and 20 mA).

To study the contact geometry between the liquid drop and molybdenum wheel, a stereomicroscope was used and attached close to the contact area. A magnified image of the contact geometry at up to 50 times was obtained.

3. Results

Sessile drop tests have shown typically poor wetting between oxide ceramics and molten metals or alloys (i.e contact angle around or greater than 90°) [11]. The results of the present wetting test showed that the contact angle varied between 140° and 160° for all the ceramics, indicating poor wetting. It was, therefore, expected that some difficulties would be encountered in the extraction of ceramic fibres. Extraction using a gas torch provided moderate temperatures (< 2000 °C). However, the heat losses from forced convection (additional to radiation loss) caused by the gas rotating with the wheel, limited the temperature capabilities of the system. Therefore, poor wetting occurred, extraction was very difficult and the product at medium to high speed mainly consisted of very small spheres. However, the laser achieved higher temperatures (2300 ± 100 °C) and so there was a significant improvement in the extraction process and ceramic fibres were obtained. Using laser heating, extraction of all molten ceramics proceeded smoothly at wheel speeds exceeding 2 m s^{-1}. However, at low wheel velocity, (i.e. ⩽ 1 m s^{-1}) no ZA fibre could be extracted.

Generally, fibres with two distinct geometries were obtained (Fig. 4). At low speeds (1.5–3 m s^{-1}), extraction initially produced uniform fibres with almost circular cross-sections depending upon the wheel tip radius. As the velocity increased beyond 4 m s^{-1} the extracted material became non-uniform. Because only

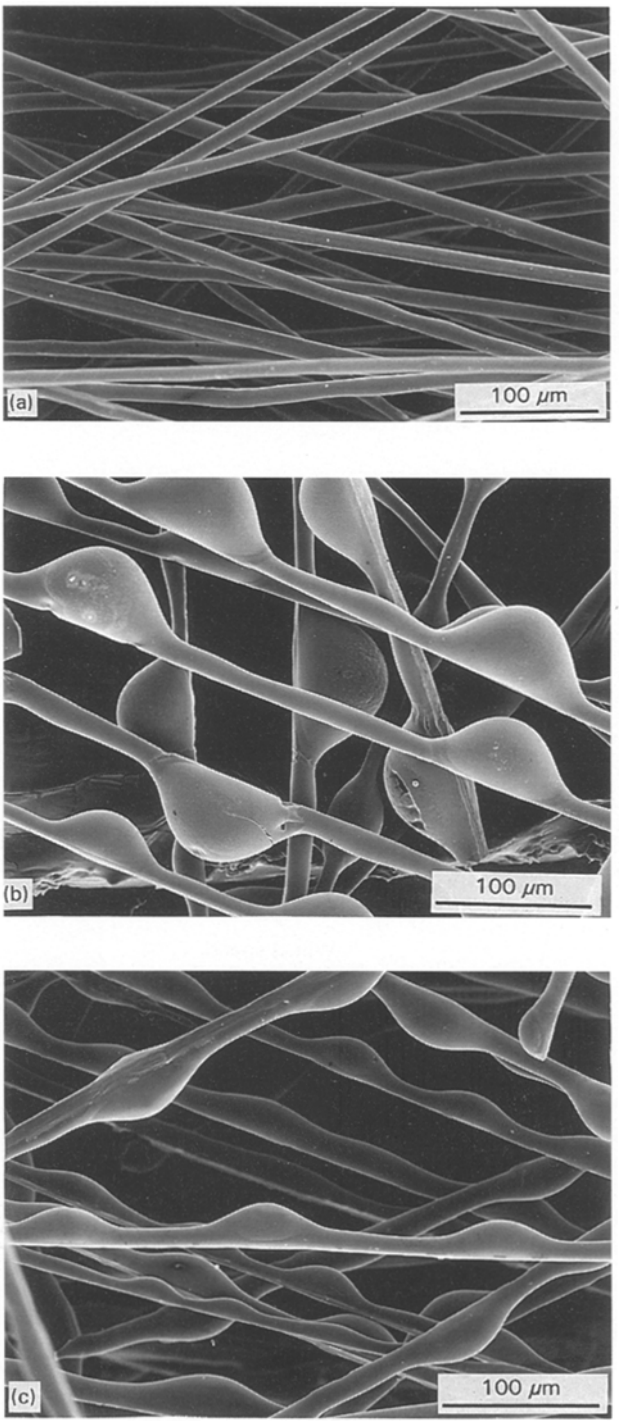

Figure 4 ZAT fibres extracted at (a) low, (b) medium, and (c) high wheel velocities (1.5, 10, and 50 m s^{-1}, respectively).

a certain thickness of the extracted layer was rapidly solidified on the wheel tip, the remaining liquid layer tended to bulge or spherodize due to the effects of surface tension and hence the shape of the extracted fibre was no longer uniform. These fibres usually consisted of a smooth thin section with periodic hemispherical balls (Rayleigh waves). The dimensions of each were designated d and h, respectively, as shown schematically in Fig. 5.

Waves start to form above a critical wheel speed ($V_1^* \approx 3$ m s^{-1}) or fibre thickness, d^*, depending upon the temperature, ceramic material, and wheel tip radius. They continued to grow up to a certain wheel speed ($V_2^* \approx 10$ m s^{-1}) and then decreased with further

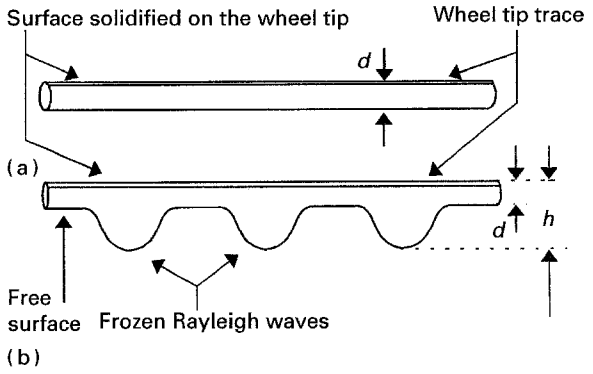

Figure 5 Schematic drawing of (a) a uniform fibre, and (b) a fibre with Rayleigh waves.

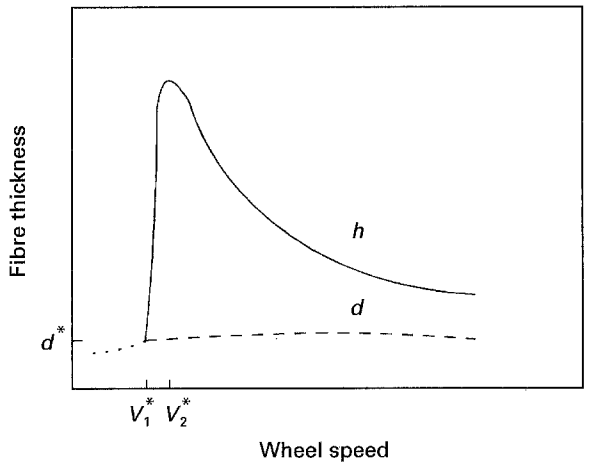

Figure 6 Typical variation of fibre thickness ((——) h and (– – –) d) versus the wheel velocity. (- - -) Smooth circular fibre.

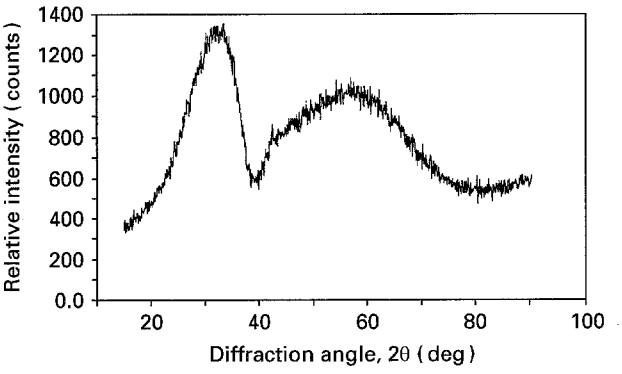

Figure 7 X-ray diffraction of fine and uniform ZAT fibres.

increase in the wheel velocity ($V > V_2^*$). Typical variations of the h and d versus wheel speed are shown in Fig. 6.

Magnified observation of the droplet in the contact with the molybdenum wheel tip indicated the details of the contact geometry, i.e. the thickness of the extracted layer and curvatures formed in dynamic wetting (see Fig. 10b below).

Very fine uniform fibres, which rapidly solidify on the wheel tip, tend to be amorphous depending upon their glass formability and thickness. Fig. 7 shows the X-ray powder diffraction pattern of ZAT fibres, indicating the amorphous nature of the fine uniform fibres.

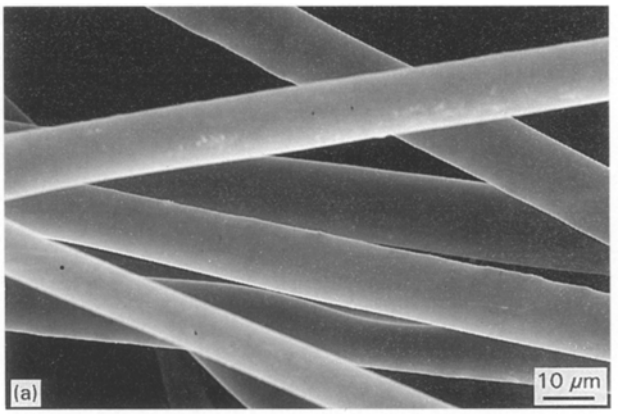

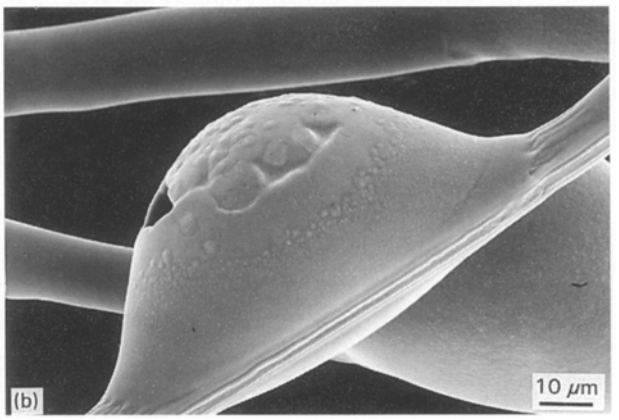

Figure 8 Surface morphology of (a) thin and (b) thick fibres.

However, with increasing fibre thickness, the mean solidification rate decreases. In fibres having Rayleigh waves, fast and slow cooling rates are experienced in the thin, d, and thick, h, sections respectively. A variety of microstructures and phases can, therefore, be obtained at various thicknesses for a given material. Fig. 8 shows the morphology of a smooth and a thick fibre. Solidification of the thick sections at lower cooling rates resulted in crystallization and defect formation as shown in Figs 8b and 4b.

4. Discussion

The governing factors in the process can be generally divided into (a) process parameters such as wetting behaviour, wheel speed, wheel tip radius, and feed rate, and (b) liquid ceramic properties, e.g. surface tension and viscosity (temperature dependent properties). Glass formability and thermal conductivity of the wheel and ceramic materials are other important parameters involved in the extraction.

Generally, the main requirement for extraction of any type of ceramic fibre is the wetting of the (molybdenum) wheel tip by the liquid ceramics. Gas heating led to the formation of tiny droplets at low temperatures and medium to high wheel speeds. This can be attributed to the poor wetting behaviour (i.e. relatively high surface tensions of the liquid ceramics and their interfaces with the molybdenum wheel tip) which hindered heat removal. Therefore, the extracted material remained liquid and became quickly spherodized into tiny particles. On the other hand, higher temperatures

and consequently lower surface tensions were achieved with laser heating. This improved the wetting between the cold molybdenum wheel tip and hot liquid ceramic, hence extraction was feasible.

During melt extraction, the characteristics of the wetting are different from the sessile drop test which is a routine test for the evaluation of wetting. In melt extraction, wetting is a dynamic process due to the rotating wheel and there is an additional shear force involved. Moreover, the wheel tip is cold whereas the sessile drop method is isothermal. These factors make the wetting behaviour in the melt extraction process quite distinct; nonetheless, we may apply the same approach as Young [12]. Fig. 9 shows of the contact geometry in static wetting (stationary wheel) and dynamic wetting. In dynamic state, the substrate is moving and a shear force, τ, is applied which is due to drag forces at the wheel/liquid interface.

In an isothermal static wetting or the sessile drop test, Young's equation for equilibrium contact angle, θ, is as follows

$$\cos(\theta) = (\gamma_{sv} - \gamma_{sl})/\gamma_{lv} \quad (1)$$

in which γ is the surface energy and subscripts of s, l, and v indicate the solid, liquid, and vapour, respectively. It should be noted that in the sessile drop test, all components are at the same temperature.

In general, wetting can be improved if γ_{sv} increases or γ_{sl} and/or γ_{lv} decreases. The surface tension of solid molybdenum (γ_{sv}) is very high because the molybdenum substrate was essentially at room temperature (note that the surface tension of molybdenum at its melting point is very high and around 2000 mJ m^{-2}, thus its surface energy at room temperature is much larger) [13]. This apparently favours the wetting behaviour because during the wetting molybdenum surface is replaced by an interface which might have lower surface energy. Another contributing factor is the surface tension of the liquid ceramics, γ_{lv}, for which data are rarely available. However, it seems that they are relatively high, e.g. the surface tension of molten alumina is around 575 mJ m^{-2} at 2200 °C [14]. It should be pointed out that high surface tension of liquid ceramics decreases wetting, whereas high surface energy of cold molybdenum improves it. However, very poor wetting was generally observed. Thus, it seems that the surface tension of the interface between the liquid ceramic and solid molybdenum, γ_{sl}, has a significant effect on wetting and large γ_{sl} results in poor wetting, which seems to be the case observed in the wetting test. Moreover, compared to an isothermal test (i.e. sessile drop test), the interfacial energy is higher because the molybdenum substrate is cold. It is suggested that γ_{sl} is so high that it limits the wetting significantly and the large contact angles (140°–160°) obtained are attributed to this fact. Generally, the wetting phenomenon in the melt extraction of ceramics is very complicated. For example, solidification of the liquid drop on the cold substrate (during spreading) plays an important role. It apparently acts as a large barrier for the liquid drop to spread on the substrate. However, an important point is why, despite having such large contact angles, melt extraction

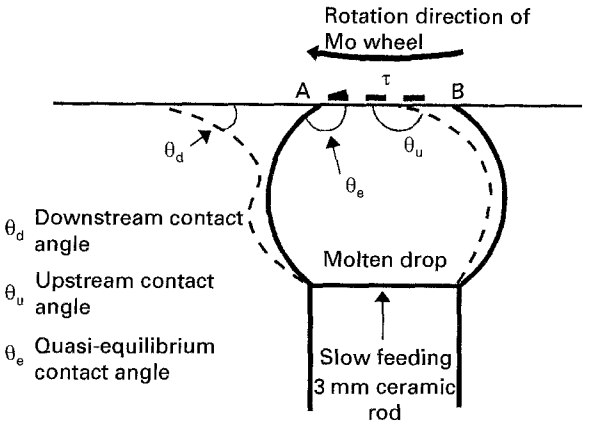

Figure 9 The wetting phenomenon in the melt extraction for (——) static and (– – –) dynamic states. A shear stress, τ, is applied at the interface in the dynamic wetting.

was feasible. This can be attributed to the rotation of the wheel which is discussed below.

Referring to Equation 1, it seems any term which increases the numerator of Equation 1, i.e. $(\gamma_{sv} - \gamma_{sl})$, also improves the wetting. Shear increases the latter because it spreads the droplet on the substrate at point A (see Fig. 9). However, on the other side of the droplet (point B), the effect of shear on wetting would be reversed. Therefore, the apparent downstream contact angle, θ_d, decreases while the apparent upstream contact angle, θ_u, increases. A decrease in the θ_d improves the wetting behaviour. The variation of contact angle, as a result of shear stress, is similar to the hysteresis of contact angle of a drop on an inclined surface [15]. Because the wetting test showed very large contact angles (i.e. poor wetting) whereas fibre extraction was achieved, it seems that shear stress has a significant effect on the enhancement of the wetting and feasibility of fibre extraction.

The extraction of ceramic fibres proceeded smoothly at wheel speeds exceeding 2 m s^{-1} for all composition studied, but at lower speeds some difficulties were encountered in extraction of ZA material. At very low-speed extraction (< 1 m s^{-1}) the shear stress is small. Therefore, it is suggested that if the surface tensions of the molten ceramic and also the interface between the hot liquid ceramic and cold molybdenum substrate are relatively low, the extraction proceeds smoothly by aid of this small shear force (e.g. extraction of ZAS, ZAT and CA fibres). On the other hand, it is difficult to extract fibres for materials which appear to have high surface energies (e.g. extraction of ZA fibre). However, as the speed increases, the shear stress at the interface increases, decreasing the downstream contract angle, and switches the process from non-wetting to wetting. Hence, a layer of the droplet is dragged out and the extraction is initiated even for high surface energy materials. We may notice that when the shear stress at the interface is large, a modified form of Equation 1, which takes into account the effect of the shear stress, cannot be applied. Under this condition the flow characteristics (not surface energies) are dominant in establishing the contact geometry including apparent contact angles. This will be further discussed below. In summary, it can be

generally said that shear at the contact surface improves the wetting and may allow fibres to be extracted despite the fact that the wetting test (Fig. 3) showed very poor wetting.

Variation of the fibre thickness versus the wheel speed (Fig. 6) can be divided into two regions; (a) very low to medium wheel speed (1–10 $m\,s^{-1}$), and (b) medium to high speed ($> 10\,m\,s^{-1}$). In the latter speed range, the fibre thickness decreases with the wheel speed and this behaviour is expected. However, in the lower speed range, increasing the wheel speed has the opposite effect on the fibre size, i.e. it increases with the wheel velocity. This is considered to be rather anomalous behaviour.

In general, as the wheel speed increases, the fibre thickness decreases. The reason is the decrease in the contact time, t (the contact length, l, over the wheel speed, V; $t = l/V$) between the wheel tip and the molten droplet. To explain the anomalous behaviour for the low-speed region, it should be pointed out that two important liquid ceramic properties are involved: surface tension and viscosity. Fundamentally, at a given speed, the thickness of the extracted layer depends upon the momentum and thermal boundary layer thicknesses or a combination of both [16]. However, it seems that in the melt-extraction of ceramic fibres, the extracted thickness is controlled by the momentum transfer because of the higher viscosity of molten ceramics and their poor thermal conductivity (compared to metals). Formation of waves also shows that the extracted layer is partially liquid after leaving the droplet. There is also evidence that thick fibres remain partially liquid even a few centimetres after leaving the wheel. Therefore, the momentum boundary layer seems to be considerably thicker than the thermal boundary layer. Magnified observation of the droplet in contact with the wheel tip showed the thickness of the extracted layer and the curvatures formed during the extraction (Fig. 10). It seems that surface tension, or the presence of curvature, r_1, tends to limit the motion of fluid as it achieves a certain momentum. In other words, momentum transfer spreads out the liquid drop while the surface tension tends to form a sphere, resisting the spreading action of the wheel. Thus, surface tension contracts the thickness of the extracted layer and consequently the fibres. Moreover, it can be inferred from these results and the literature [16] that as the speed increases, the effect of surface tension gradually diminishes, while the viscosity, through which the shear force penetrates, becomes more dominant. In other words, for medium to high wheel velocities the effect of surface tension becomes negligible compared to viscosity in controlling the thickness of the extracted layer. Therefore, the governing material parameter in the declining region of Fig. 6 (i.e. $V > V_2^*$) is the viscosity of the liquid ceramic. Inverarity [17] suggested that the description of the dynamic contact angle was mainly viscosity-dependent and indicated that surface tension was relatively unimportant in a system of high-speed dynamic wetting.

Variation of fibre thickness with the wheel speed can also be altered by the feed rate. However, as

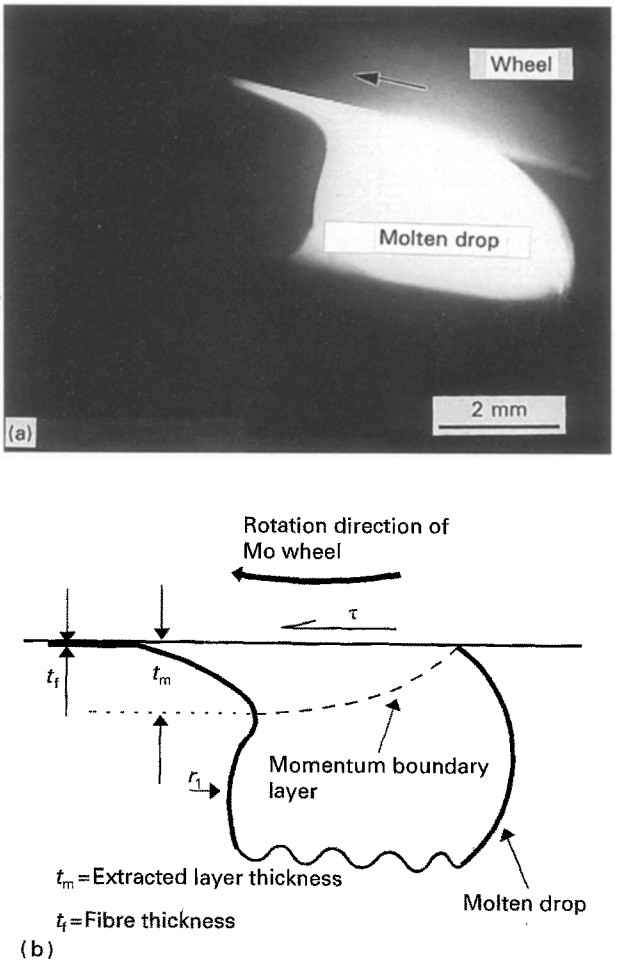

Figure 10 Magnified contact geometry of the liquid droplet and the molybdenum wheel tip. (a) Real contact geometry, and (b) a schematic showing the imaginary momentum boundary layer and the thickness of the extracted layer and fibre.

mentioned, it is crucial to maintain the temperature of the molten droplet on the ceramic rod constant because any variation would affect the surface tension and viscosity of the liquid ceramic. Therefore, the feed rate of the ceramic rod was kept constant, regardless of the wheel velocity. It should be pointed out that this can change the geometry of the contact area which, in turn, affects the fibre thickness. Therefore, as the speed increases, it appears that the area of contact and the thickness of the extracted fibre decrease concurrently. Nonetheless, the fibre thickness initially increases and then decreases which implies that the change in the contact area is probably not significant. It is, therefore, suggested that even if the feed rate is changed so as to maintain the ratio of the feed rate to the wheel speed constant, then the same type of curve, as shown in Fig. 6, would be obtained.

Fibre geometry is also affected by the surface energy of liquid ceramics. Although, as already mentioned, the effect of surface tension on controlling the extracted layer thickness diminishes as the wheel speed increases, it definitely affects the fibre geometry regardless of the speed. Indeed, the formation of the fine fibres with almost circular cross-sections at low-speed (1–3 $m\,s^{-1}$) and Rayleigh waves at wheel speeds exceeding 4 $m\,s^{-1}$ on the free side of the fibres is governed by the surface tension of the liquid ceramic.

Surface tension of a liquid tends to minimize the surface area because low surface area is energetically favourable. Therefore, circular cross-section fibres and Rayleigh waves are quickly formed to reduce the exposed surface area.

This phenomenon is well known for a jet of a liquid [18]. In this case, surface tension destabilizes the jet stream and finally it breaks up the jet into fine droplets. The Rayleigh waves formed on a liquid stream before its break-up are well-known and documented [19]. In the melt-extraction process, because solidification is simultaneously occurring with extraction (provided there is enough wetting), the destabilizing effect of surface tension cannot result in fibre or stream break-up. Hence, frozen Rayleigh waves are seen on the free side of the extracted fibres (Figs 4 and 5). It should be pointed out that during extraction using gas heating, the wetting was so poor that almost no solidification occurred in contact with the wheel. In this case, the Rayleigh instabilities grew to such an extent that they caused the extracted layer to disintegrate and so small spheres were formed rather than a continuous fibre.

The critical speed to start forming Rayleigh waves, V_1^*, depends on the temperature, because controlling parameters, i.e. surface tension and viscosity are temperature dependent. Wheel-tip radius and immersion depth of the wheel tip into the liquid droplet also alter V_1^*. Rayleigh waves are formed when the speed or the fibre thickness exceeds a certain limit ($V > V_1^*$ or $d > d^*$). In this case, an extracted fibre is partially solid while travelling on the wheel tip or upon leaving it. Because the solidification rate drops as the fibre thickness increases, the cooling rate is not high enough to solidify the whole fibre immediately. The surface tension then dominates and forms the Rayleigh instabilities. The thicker the extracted material, the larger are the Rayleigh waves formed on the fibre-free surface.

Fig. 6 shows that h varies significantly with the wheel speed, while d remains more or less constant. It is thought that this thickness, d, is mainly controlled by the rapid solidification of the extracted layer on the wheel tip before it starts to flow under the effect of surface tension and to form Rayleigh waves. For a given wetting behaviour, it seems that three factors determine the value of d and are as follows: (a) the thermal conductivity of the liquid and solid ceramic, (b) the wheel tip radius, and (c) the depth of wheel tip immersion into the liquid droplet. The relatively low thermal conductivity of ceramics, small wheel tip radius, and shallow depth of immersion decrease the value of d and vice versa.

Once Rayleigh waves are formed, the fibres no longer exhibit uniform shape hence various cooling rates are experienced in the thin and thick sections. Therefore, a variety of microstructures can be obtained (Figs 4 and 8). Cooling rate is governed by the heat-transfer mechanism which, for fine uniform fibres, is predominantly conduction. However, if solidification of the almost whole extracted layer does not occur sufficiently fast or a ceramic fibre leaves the wheel tip while it is still partially liquid, the dominant heat-transfer mechanism changes from conduction to a combination of conduction and radiation. This, in turn, decreases the cooling rate of the extracted layer. Therefore, the liquid layer forms waves, and low and high cooling rates are experienced, in the thick and thin sections of the fibres respectively. Slow cooling rates in the thick regions increase the probability of crystallization. Significant shrinkage is associated with ceramic crystallization, and it is accompanied by the formation of porosity and cracks depending upon the cooling rate and is illustrated in Fig. 8b.

5. Conclusion

Melt-extracted oxide ceramic fibres can be produced using an oxy-fuel torch, and/or a CO_2 laser, and a sharp molybdenum wheel. The main requirement in the process is wetting between the extraction wheel tip and molten ceramics. A specially designed wetting test which simulates the transient wetting behaviour occurring during the melt extraction showed that there was poor wetting in the process. However, the presence of a shear force at the interface between the liquid droplet and the molybdenum wheel tip improved the dynamic wetting and initiated the extraction process. Extracted fibres at low speed were uniform, but with increasing extraction speed, the fibres became thicker and Rayleigh instabilities formed on the free side of the fibres.

An anomalous behaviour of fibre thickness versus the wheel velocity was obtained for low wheel speeds ($< 10\ m\ s^{-1}$). This behaviour is related to the competing effects of the surface tension and viscosity. Surface tension tends to restrict the thickness of the extracted layer and this can be seen especially at low speed ($< 10\ m\ s^{-1}$). However, at moderate to high speed ($> 10\ m\ s^{-1}$), surface tension has a negligible effect on the thickness of the extracted layer compared to the viscosity effect. Therefore, for this range of speeds, the extracted layer thickness, which is believed to be governed by momentum transfer, is basically controlled by the liquid ceramic viscosity. Thus, an increase in the wheel velocity decreases the contact time and consequently the extracted layer and fibre thicknesses. Formation of thin and thick sections in fibres is associated with high and low cooling rates. Therefore, a variety of microstructures can be obtained.

Acknowledgements

The authors acknowledge the support of this research through a NSERC Strategic Grant and financial support of Ceramatrix Inc., Montreal, Canada. M. Allahverdi thanks the Iranian Ministry of Culture and Higher Education, for a scholarship.

References

1. P. BRACKE, H. SCHURMANS and J. VERHOEST, "Inorganic Fibers and Composite Materials, a Survey of Recent Development" (Pergamon International Information Incorporation, Netherlands, 1984) pp. 11, 35, 49.

2. K. K. CHAWLA, "Composite Materials- Science and Technology" (Springer, New York, 1987) p. 102.
3. R. E. MARINGER, A. RUDNICK and C. E. MOBLEY, US Pat. 3838185, 24 September 1974.
4. R. E. MARINGER and C. E. MOBLEY, *J. Vac. Sci. Technol.* **11** (1974) 1067.
5. O. M. STEWART, R. E. MARINGER and C. E. MOBLEY, US Pat. 3812901, 28 May 1974.
6. R. E. MARINGER and C. E. MOBLEY, in "Proceedings of 3rd International Conference on Rapidly Quenched Metals", RQ 78, edited by B. Cantor (The Metals Society, London, 1978) p. 49.
7. L. A. SCHWARTZKOPF, J. E. OSTENSEN and D. K. FINNEMORE, US Pat. 4970194, 13 November 1990.
8. L. A. SCHWARTZKOPF, US Pat. 5053384, 1 October 1991.
9. P. BOSSWELL, D. RICHTER, T. BERCE and G. NEGATY-HINDI, US Pat. 5067554, 26 November 1991.
10. J. O. STROM-OLSEN, G. RUDKOWSKI, P. RUDKOWSKA, M. ALLAHVERDI and R. A. L. DREW, *Mater. Sci. Eng.* **A179/A180** (1994) 158.
11. JU. V. NADIACH, in "Progress in Surface and Membrane Science", Vol. 14, edited by D. A. Cadenhead and J. F. Danielli (Academic Press, New York, 1981) p. 380.
12. T. YOUNG, *Trans. R. Soc. Lond.* **95** (1805) 65.
13. D. R. LIDE (ed.) "Handbook of Chemistry and Physics", 72nd Edn (CRC Press, Boston, 1991–1992) pp. 4–138.
14. V. P. ELYUTIN, B. S. MITIN and YU. S. ANISIMOV, *Izv. Vyssh. Uchebn. Zaved, Tsventn. Metall.* **17** (1974) 42.
15. E. WOLFRAM and R. FAUST, in "Wetting, Spreading, and Adhesion", edited by J. F Padday (Academic Press, New York 1978) p. 213.
16. S. KAVESH, "Metallic Glasses" (American Society for Metals, Metals Park, OH, 1978) p. 36.
17. G. INVERARITY, *Br. Polymer J.* **1** (1969) 245.
18. R. D. REITZ and F. V. BRACCO, in "Encyclopedia of Fluid Mechanics", Vol. 3, "Gas-Liquid Flows", edited by Nicholas P. Cheremisinoff (Gulf Houston, TX, 1986) Ch. 10, p. 233.
19. R. E. CUNNINGHAM, L. E. RAKSTRAW and S. A. DUNN, *AiChE,' Sym. Ser. No. [180]* **74** (1978) 20.

Received 7 July 1994
and accepted 16 August 1995